

# ExSample: Efficient Searches on Video Repositories through Adaptive Sampling

Oscar Moll  
MIT CSAIL

orm@csail.mit.edu

Mike Stonebraker  
MIT CSAIL

stonebraker@csail.mit.edu

Favyen Bastani  
MIT CSAIL

favyen@csail.mit.edu

Vijay Gadepally  
MIT Lincoln Laboratory

vijayg@ll.mit.edu

Sam Madden  
MIT CSAIL

madden@csail.mit.edu

Tim Kraska  
MIT CSAIL

kraska@mit.edu

## ABSTRACT

Capturing and processing video is increasingly common as cameras become cheaper to deploy. At the same time, rich video understanding methods have progressed greatly in the last decade. As a result, many organizations now have massive repositories of video data, with applications in mapping, navigation, autonomous driving, and other areas.

Because state-of-the-art object detection methods are slow and expensive, our ability to process even simple ad-hoc object search queries (“find 100 traffic lights in dashcam video”) over this accumulated data lags far behind our ability to collect it. Processing video at reduced sampling rates is a reasonable default strategy for these types of queries, however, the ideal sampling rate is both data and query dependent. We introduce ExSample, a low cost framework for object search over un-indexed video that quickly processes search queries by adapting the amount and location of sampled frames to the particular data and query being processed.

ExSample prioritizes the processing of frames in a video repository so that processing is focused in portions of video that most likely contain objects of interest. It continually re-prioritizes processing based on feedback from previously processed frames. On large, real-world datasets, ExSample reduces processing time by up to 6x over an efficient random sampling baseline and by several orders of magnitude over state-of-the-art methods that train specialized per-query surrogate models. ExSample is thus a key component in building cost-efficient video data management systems.

### PVLDB Reference Format:

xxx. xxx. *PVLDB*, 21(xxx): xxxx-yyyy, 2021.  
DOI: <https://doi.org/10.14778/xxxxxxx.xxxxxxx>

## 1. INTRODUCTION

Video cameras have become incredibly affordable over the last decade, and are ubiquitously deployed in static and mobile settings, such as smartphones, vehicles, surveillance

This work is licensed under the Creative Commons Attribution-NonCommercial-NoDerivatives 4.0 International License. To view a copy of this license, visit <http://creativecommons.org/licenses/by-nc-nd/4.0/>. For any use beyond those covered by this license, obtain permission by emailing [info@vldb.org](mailto:info@vldb.org). Copyright is held by the owner/author(s). Publication rights licensed to the VLDB Endowment.

*Proceedings of the VLDB Endowment*, Vol. 21, No. xxx  
ISSN 2150-8097.

DOI: <https://doi.org/10.14778/xxxxxxx.xxxxxxx>

cameras, and drones. Large video datasets are enabling a new generation of applications. For example, video data from vehicle dashboard-mounted cameras (dashcams) is used to train object detection and tracking models for autonomous driving systems [35]; to annotate map datasets like OpenStreetMap with locations of traffic lights, stop signs, and other infrastructure [26]; and to analyze collision scenes in dashcam footage to automate insurance claims processing [28].

However, these applications must process large amounts of video to extract useful information. Consider the task of finding examples of traffic lights – to, for example, annotate a map – within a large collection of dashcam video collected from many vehicles. The most basic approach to evaluate this query is to run an object detector frame by frame over the dataset. Because state-of-the-art object detectors run at about 10 frames per second (fps) over 1080p video on modern high-end GPUs, scanning through a collection of 1000 hours of 30 fps video with a detector on a GPU would take 3000 GPU-hours. In the offline query case, which is the case we focus on in this paper, we can parallelize our scan over the video across many GPUs, but, as the rental price of a GPU is around \$0.50 per hour (for the cheapest *g4* AWS instance in 2020) [1], our bill for this one ad-hoc query would be \$1.5K, regardless of parallelism. Hence, this workload presents challenges in both time and monetary cost. Note that accumulating 1000 hours of video represents just 10 cameras recording for less than a week.

A straightforward means for mitigating this issue is to reduce the number of sampled frames: for example, only run the detector on one frame per second of video. After all, we might think it reasonable to assume all traffic lights are visible for longer than one second. The savings are large compared to inspecting every frame: processing only one frame every second decreases costs by 30x for a video recorded at 30 fps. Unfortunately, this strategy has limitations: for example, the one frame out of every 30 that we look at may not show the light clearly, causing the detector to miss it completely. Second, lights that remain visible in the video for long intervals, like 30 seconds, would be seen multiple times unnecessarily, thereby wasting resources detecting those objects repeatedly. Worse still, we may miss other types of objects that remain visible for shorter intervals, and in general the optimal sampling rate is unknown, and varies across datasets depending on factors such as whether the camera is moving or static, and the angle and distance to the object.

In this paper, we introduce ExSample, a video sampling

technique designed to reduce the number of frames that need to be processed by an expensive object detector for object search queries over large video repositories. ExSample models this problem as one of deciding which frame from the dataset to look at next based on what it has seen in the past. Specifically, ExSample splits the dataset into temporal chunks (e.g. half-hour chunks), and maintains a per-chunk estimate of the probability of finding a new object in a frame randomly sampled from that chunk. ExSample iteratively selects the chunk with the best estimate, samples a frame randomly from the chunk, and processes the frame through the object detector. ExSample updates the per-chunk estimates after each iteration so that the estimates become more accurate as more frames are processed.

Recent state-of-the-art methods for optimizing queries over large video repositories have focused on training cheap, surrogate models to approximate the outputs of expensive, deep neural networks [2, 12, 18, 20, 24]. In particular, BlazeIt [17] adapts such surrogate-based methods for object search limit queries, and optimizes these queries by training a lightweight surrogate model to output high scores on frames containing the object of interest and low scores on other frames; BlazeIt computes scores through the surrogate over the entire dataset, and then prioritizes high-scoring frames for processing through the object detector. However, this approach has two critical shortcomings, which we expand on in Section 2.2. First, even when processing limit queries, where the user seeks a fixed number of results, BlazeIt still requires a time-consuming upfront dataset scan in order to compute surrogate scores on every video frame. Second, while frames with high surrogate scores are likely to contain object detections relevant to a query, those objects may have already been seen in neighboring frames earlier during processing, and so applying the object detector on those frames does not yield new objects.

ExSample addresses the aforementioned shortcomings to achieve an order of magnitude speedup over the prior state-of-the-art (BlazeIt). First, rather than select frames for applying the object detector based on surrogate scores, ExSample employs an adaptive sampling technique that eliminates the need for a surrogate model and an upfront full scan. A key challenge here is that, in order to generalize across datasets and object types, ExSample must not make assumptions about how long objects remain visible to the camera and how frequently they appear. To address this challenge, ExSample guides future processing using feedback from object detector outputs on previously processed frames. Second, ExSample gives higher weight to portions of video likely to not only contain objects, but also to contain objects that haven’t been seen already. Thus, ExSample avoids redundantly processing frames that only contain detections of objects that were previously seen in other frames.

We evaluate ExSample on a variety of search queries spanning different objects, different kinds of video, and different numbers of desired results. We show savings in the number of frames processed ranging up to 6x on real data, with a geometric average of 2x across all settings, in comparison to an efficient random sampling baseline. In the worst case, ExSample does not perform worse than `random` sampling, something that is not always true of alternative approaches. Additionally, in comparison to BlazeIt [17], our method processes fewer frames to find the same number of distinct results in many cases, showing that ExSample provides higher

precision than a surrogate model in selecting frames with new objects; even in the remaining cases, ExSample still requires one to two-orders of magnitude less runtime (or, equivalently, dollar cost) because it does not require an upfront per-query scan of the entire dataset.

In summary, our contributions are (1) ExSample, an adaptive sampling method that facilitates ad-hoc object searches over video repositories, (2) a formal analysis of ExSample’s design, and (3) an empirical evaluation showing ExSample is effective on real datasets and under real system constraints, and that it outperforms existing approaches for object search.

## 2. BACKGROUND

In this section we review object detection, introduce distinct object queries, and discuss limitations of prior work.

### 2.1 Object Detection

An object detector is a model that operates on still images, inputting an image and outputting a set of boxes within the image containing the objects of interest. The amount of objects found will range from zero to arbitrarily many. Well known examples of object detectors include Yolo [31] and Mask R-CNN [10]. In Figure 1, we show two example frames that have been processed by an object detector, with yellow boxes indicating detections of traffic lights.

Object detectors with state-of-the-art accuracy in benchmarks such as COCO [23] typically execute at around 10 frames per second on modern GPUs, though it is possible to achieve real time rates by sacrificing accuracy [13, 31].

In this paper we do not seek to improve on state-of-the-art object detection approaches. Instead, we treat object detectors as a black box with a costly runtime, and aim to substantially reduce the number of video frames that need to be processed by the detector.

### 2.2 Distinct Object Queries

In this paper, we are interested in processing higher level queries on video enabled by the availability of object detectors. In particular, we are concerned with distinct object limit queries such as “find 20 traffic lights in my dataset” over large repositories of multiple videos from multiple cameras. For distinct object queries, each result should be a detection of a different object. For example, in Figure 1, we detected the same traffic light in two frames several seconds apart; although these detections are at different positions and are computed in different frames, in a distinct object query, these two detections yield only one distinct result.



Figure 1: Two video frames showing the same traffic light instance several seconds apart. A distinct object query is defined by having these two boxes only count as one result.

Then, to specify a query, users must specify not only the object type of interest and the number of desired results, but also a *discriminator function* that determines whether a new detection corresponds to an object that was already

seen earlier during processing. In this paper, we assume a fixed discriminator that applies an object tracking algorithm to determine whether a detection is new: it applies a tracker similar to SORT [3] backwards and forwards through video for each detection of a new object to compute the position of that object in each frame where the object was visible; then, future detections are discarded if they match previously observed positions.

The goal of this paper is to reduce the cost of processing such queries. Moreover, we want to do this on ad-hoc distinct object queries over large video repositories, where there are diverse videos in our dataset and where it is too costly to compute all object detections ahead of time for the type of objects we are looking for. This distinction affects multiple decisions in the paper, including not only the results we return but also the main design of ExSample and how we measure result recall.

Below, we discuss two baselines and prior work for optimizing the processing of distinct object queries.

**Naive execution.** A straightforward method is to process frames sequentially, applying the object detector on each frame of each video, using the discriminator function to discard repeated detections of the same object. Once we collect enough distinct objects to satisfy the query’s limit clause, we can stop scanning. A natural extension is to sample only 1 out of every  $n$  frames. Sequential processing exhibits high variance in execution time due to the uneven distribution of objects in video. Moreover, if objects appear in the video for much longer than the sampling rate, we may repeatedly compute detections of the same object. Similarly, if objects appear for shorter than the sampling rate, we may completely miss some objects.

**Random sampling.** A better strategy is to iteratively process frames uniformly sampled from the video repository (without replacement). This method reduces the query execution time over naive execution as it explores more areas of the data more quickly, whereas sequential execution can get stuck in a long segment of video with no objects. Additionally, early in query execution, randomly sampled frames are less likely to contain previously seen objects compared to frames sampled sequentially.

**Surrogate-based methods.** Methods that optimize video query execution by training cheap, surrogate models to approximate the outputs of expensive object detectors have recently attracted much interest. In particular, BlazeIt [17] proposes an adaption of surrogate model techniques for processing distinct object queries with limit clauses: rather than randomly sampling frames for processing through the object detector, BlazeIt processes frames in order of the score computed by the surrogate model on the frame, beginning with the highest scoring frames. Since the surrogate model is trained to produce higher scores on frames containing relevant object detections, this approach effectively ensures that frames processed early during execution contain relevant detections (but not necessarily new objects).

However, surrogate-based methods have several critical shortcomings when used for processing object search queries. First, for queries seeking rare objects that appear infrequently in video, these methods require substantial pre-processing to collect annotations for training the surrogate models, which can be as costly as solving the search problem in the first place; indeed, BlazeIt resorts to random

sampling if the number of positive training labels is too small. Moreover, when processing limit queries, surrogate-based methods require an upfront per-query dataset scan in order to compute surrogate scores on every video frame in the dataset. As we will show in our evaluation, oftentimes, the cost of performing just this scan is already larger than simply processing a limit query under random sampling.

### 3. ExSample

In this section we explain how our approach, ExSample, optimizes query execution. Due to the high compute demand of object detectors, runtime in ExSample is roughly proportional to the number of frames processed by the detector. Thus, we focus on minimizing the number of frames processed to find some number of distinct objects.

To do so, ExSample estimates which portions of a video are more likely to yield new results, and samples frames more often from those portions. Importantly, ExSample prioritizes finding distinct objects, rather than purely maximizing the number of computed object detections.

At a high level, ExSample conceptually splits the input into chunks, and scores each chunk separately based on the frequency with which distinct objects have been found in that chunk in the past. This scoring system allows ExSample to allocate resources to more promising chunks while also allowing it to diversify where it looks next over time. In our evaluation, we show that this technique helps ExSample outperform greedy surrogate-guided strategies, even when they employ duplicate avoidance heuristics (i.e., do not process frames that are close to previously processed frames).

To make it practical, ExSample is composed of two core components: an estimate of future results per chunk, described in Section 3.1, and a mechanism to translate these estimates into a sampling decision which accounts for estimate errors, introduced in Section 3.4. In those two sections we focus on quantifying the types of error. Later, in Section 3.5, we detail the algorithm step by step.

#### 3.1 Scoring a Single Chunk

In this section we derive our estimate for the future value of sampling a chunk. To make an optimal decision of which chunk to sample next, assuming  $n$  samples have been taken already, ExSample estimates  $R(n+1)$  for each chunk, which represents the number of *new* results we expect to find on the next sample. *New* means  $R$  does not include objects already found in the previous  $n$  samples, even if they appeared also in the  $(n+1)^{\text{th}}$  frame. Intuitively, the chunk with the largest  $R(n+1)$  is a good location to pick a frame from next.

Let  $N$  be the number of distinct objects in the data. Each object  $i$  out of those  $N$  will be visible for a different number of frames, which means that when sampling frames at random from a chunk, each  $i$  will have a different probability of being found, which we call  $p_i$ . For example, in video collected from a moving vehicle that stops at a red light, red lights will tend to have large  $p_i$  lasting in the order of minutes, while green and yellow lights are likely to have much smaller  $p_i$ , perhaps in the order of a few seconds. We find that in practice these  $p_i$  vary widely even for a single object class, from tens to thousands of frames.

We emphasize that  $p_i$  and  $N$  are not known in advance and neither the user nor ExSample knows them, instead, ExSample relies on estimating the sum  $R(n+1) = \sum_{i=1}^N p_i \cdot [i \notin \text{seen}(n)]$  without estimating  $N$  and the  $p_i$  directly.

The estimate is similar to the Good-Turing estimator [7], and relies on counting the number of distinct objects seen exactly once so far, which we denote  $N^1(n)$ . That is, after sampling a frame and seeing a new object for the first time,  $N^1(n)$  increases by 1, and after observing the same object a second time in a different frame,  $N^1(n)$  decreases by 1. Unlike the  $p_i$  or  $N$ , which are unknown to the user and to ExSample,  $N^1(n)$  is a quantity we can observe and track as we sample frames. For a single chunk, our estimate is:

$$R(n+1) \approx N^1(n)/n \quad (1)$$

This formula is similar to the Good-Turing estimator [7], but under a different setting where the meaning of  $N^1(n)$  is somewhat different. Specifically, in object search over video, we sample frames rather than symbols at random, and so a single frame can contain many objects, or no object at all. This means that in ExSample,  $N$  and  $N^1(n)$  could range from 0 to far larger than  $n$  itself, e.g. in a crowded scene with many distinct objects per frame. In the traditional use of the Good-Turing estimator (such as the one explained in the original paper [7]) there is exactly one instance per sample and the only question is whether it is new. In that situation  $N^1(n)$  will always be smaller than  $n$ .

In the following sub-sections, we describe the bias and variance of the estimate in terms of  $n$ ,  $N$ , the average duration of a result  $\mu_p = \sum p_i/N$  and also the standard deviation of the  $p_i$   $\sigma_p$ .

In particular we first will bound the relative bias:

$$\text{rel. err} = \frac{E[N^1(n)]/n - E[R(n+1)]}{E[N^1(n)]/n}$$

The following inequalities bound the relative bias error of our estimate:

**Theorem (Bias).**

$$0 \leq \text{rel. err} \quad (2)$$

$$\text{rel. err} \leq \max p_i \quad (3)$$

$$\text{rel. err} \leq \sqrt{N}(\mu_p + \sigma_p) \quad (4)$$

Intuitively, (2) implies that  $N^1(n)/n$  tends to overestimate  $R(n+1)$ , (3) implies that the size of the overestimate is guaranteed to be less than the largest probability, which is likely small, and (4) implies that even if a few  $p_i$  outliers were large, as long the durations within one standard deviation  $\sigma_p$  of the average  $\mu_p$  are small the error will remain small. A large  $N$  or a large  $\mu_p$  or  $\sigma_p$  may seem problematic for Equation 4, but we note that a large number of results  $N$  or long average duration  $\mu_p$  implies many results will be found after only a few samples, so the end goal of the search problem is easy in the first place and having guarantees of accurate estimates is less important.

In later experiments, we will show that we consistently perform well both in simulated skewed data containing many objects, and in five real-world datasets with diverse skews.

*Proof.* Now we prove Equation 2 Equation 3, and Equation 4. The chance that object  $i$  is seen on the  $(n+1)^{\text{th}}$  random sample from the chunk after being missed on the

first  $n$  samples is  $p_i(1-p_i)^n$ . For the rest of the paper, we denote this quantity  $\pi_i(n+1)$ . By linearity of expectation:

$$E[R(n+1)] = \sum_{i=1}^N \pi_i(n+1)$$

For the rest of this proof, we will avoid explicitly writing summation indexes  $i$ , since our summations always are over the result instances, from  $i=0$  to  $N$ .

$E[N^1(n)]$  can also be expressed directly. The chance of having seen instance  $i$  exactly once after  $n$  samples is  $np_i(1-p_i)^{n-1}$ , with the extra  $n$  coming from the possibility of the instance having shown up at any of the first  $n$  samples. We can rewrite this as  $n\pi_i(n)$ . So  $E[N^1(n)] = n\sum\pi_i(n)$ , giving:

$$E[N^1(n)]/n = \sum\pi_i(n)$$

Now we will focus on the numerator  $E[N^1(n)]/n - R(n+1)$

$$\begin{aligned} E[N^1(n)]/n - E[R(n+1)] &= \sum\pi_i(n) - \pi_i(n+1) \\ &= \sum p_i^2(1-p_i)^{n-1} \\ &= \sum p_i\pi_i(n) \end{aligned}$$

We can see here that each term in the error is positive, hence we always overestimate, which proves Equation 2.

Now bound this overestimate. Intuitively, this overestimate is small because each term is a scaled down version of the terms in  $E[N^1(n)]/n = \sum\pi_i(n)$ , more precisely:

$$\begin{aligned} \sum p_i\pi_i(n) &\leq (\max p_i) \cdot \sum\pi_i(n) \\ &= (\max p_i) \cdot E[N^1(n)]/n \end{aligned} \quad (5)$$

For example, if all the  $p_i$  are all less than 1%, then the overestimate is also less than 1% of  $N^1(n)/n$ . However, if we know there may be a few outliers with large  $p_i$  which are not representative of the rest, unavoidable in real data, then we would like to know our estimate will still be useful. We can show this is still true as follows:

$$\begin{aligned} \sum p_i\pi_i(n) &\leq \sqrt{(\sum p_i^2)(\sum \pi_i^2)} && \text{(Cauchy-Schwarz)} \\ &\leq \sqrt{(\sum p_i^2)(\sum \pi_i)^2} && \pi_i \text{ are positive} \\ &= \sqrt{(\sum p_i^2)\sum \pi_i} \\ &= \sqrt{(\sum p_i^2)E[N^1]/n} \\ &= \sqrt{N}\sqrt{(\sum p_i^2/N)E[N^1]/n} \end{aligned}$$

The term  $\sum p_i^2/N$  is the second moment of the  $p_i$ , and can be rewritten as  $\sigma_p^2 + \mu_p^2$ , where  $\mu_p$  and  $\sigma_p$  are the mean and standard deviation of the underlying result durations:

$$\begin{aligned} &= \sqrt{N}\sqrt{(\sigma_p^2 + \mu_p^2)E[N^1]/n} \\ &\leq \sqrt{N}(\sigma_p + \mu_p)E[N^1]/n \end{aligned} \quad (6)$$

Putting together Equation 5 and Equation 6 we get:

$$E[N^1(n)]/n - E[R(n+1)] \leq \begin{cases} (\max p_i) \frac{E[N^1]}{n} \\ \sqrt{N}(\sigma_p + \mu_p) \frac{E[N^1]}{n} \end{cases}$$

And dividing both sides, we get

$$\text{rel. err} = \frac{E[N^1(n)]/n - E[R(n+1)]}{E[N^1(n)]/n} \leq \begin{cases} \max p_i \\ \sqrt{N}(\sigma_p + \mu_p) \end{cases}$$

Which justifies the remaining two bounds: Equation 3 and Equation 4.  $\square$

### 3.2 Scoring Multiple Chunks

If we knew  $R_j(n_j + 1)$  for every chunk  $j$ , the algorithm could simply take the next sample from the chunk with the largest estimate. However, if we simply use the raw estimate:

$$R_j(n_j + 1) \approx N_j^1(n_j)/n_j \quad (7)$$

And pick the chunk with the largest estimate, then we run into two potential problems. First, instances may span multiple chunks. This corner case can be handled easily by adjusting the definition of  $N_j^1$ , and can be verified directly in a similar way to Equation 1 (see our technical report [25]). Moreover, each chunk's estimate may be off due to the random sample error, especially in chunks with small  $n_j$ , which we handle next.

### 3.3 Instances spanning multiple chunks

If instances span multiple chunks, for example a traffic light that spans across the boundaries of two neighboring chunks, Equation 7 is still accurate with the caveat that  $N_j^1(n_j)$  is interpreted as the number of instances seen exactly once *globally* and which were found in chunk  $j$ . The same object found once in two chunks  $j$  and  $k$  does not contribute to either  $N_j^1$  or to  $N_k^1$ , even though each chunk has only seen it once. The derivation of this rule is similar to that in the previous section, and is given in Section 3.3. In practice, if only a few rare instances span multiple chunks then results are almost the same and this adjustment does not need to be implemented.

At runtime, the numerator  $N_j^1$  will only increase in value the first time we find a new result globally, decrease back as soon as we find it again either in the same chunk or elsewhere, and finding it a third time would not change it anymore. Meanwhile  $n_j$  increases upon sampling a frame from that chunk. This natural relative increase and decrease of  $N_j^1$  with respect to each other allows ExSample to seamlessly shift where it allocates samples over time.

Here we prove Equation 7 is also valid when different chunks may share instances. Assume we have sampled  $n_1$  frames from chunk 1,  $n_2$  from chunk 2, etc. Assume instance  $i$  can appear in multiple chunks: with probability  $p_{i1}$  of being seen after sampling chunk 1,  $p_{i2}$  of being seen after sampling chunk 2 and so on. We will assume we are working with chunk 1, without loss of generality. The expected number of new instances if we sample once more from chunk 1 is:

$$R_1(n+1) = \sum_{i=1}^N \left[ p_{i1}(1-p_{i1})^{n_1} \prod_{j=2}^M (1-p_{ij})^{n_j} \right] \quad (8)$$

Similarly, the expected number of instances seen exactly once in chunk 1, and in no other chunk up to this point is

$$N_1^1 = \sum_{i=1}^N \left[ n_1 p_{i1} (1-p_{i1})^{n_1-1} \prod_{j=2}^M (1-p_{ij})^{n_j} \right] \quad (9)$$

In both equations, the expression  $\prod_{j=2}^M (1-p_{ij})^{n_j}$  factors in the need for instance  $i$  to not have been while sampling chunks 2 to  $M$ . We will abbreviate this factor as  $q_i$ . When

instances only show up in one chunk,  $q_i = 1$ , and everything is the same as in Equation 1.

The expected error is:

$$N_1^1(n_1)/n_1 - R_1(n_1+1) = \sum_{i=1}^N [p_{i1}^2(1-p_{i1})^{n_1-1}q_i] \quad (10)$$

Which again is term-by-term smaller than  $N_1^1(n_1)/n_1$  by a factor of  $p_i$

### 3.4 Sampling Chunks Under Uncertainty

Before we develop our sampling method, we need to handle the problem that an observed  $N^1(n)$  will fluctuate randomly due to randomness in our sampling. This is especially true early in the sampling process, where only a few samples have been collected but we need to make a sampling decision. Because the quality of the estimates themselves is tied to the number of samples we have taken, and we do not want to stop sampling a chunk due to a small amount of bad luck early on, it is important we estimate how noisy our estimate is. The usual way to do this is by estimating the variance of our estimator:  $\text{Var}[N^1(n)/n]$ . Once we have a good idea on how this variance error depends on the number of samples taken, we can derive our sampling method, which balances both the raw estimate of new objects and the number of samples it is based on.

**Theorem (Variance).** *If instances occur independently of each other, then*

$$\text{Var}[N^1(n)/n] \leq \text{E}[N^1(n)]/n^2 \quad (11)$$

Note that this bound also implies that the variance error is more than  $n$  times smaller than the value of the raw estimate, because we can rewrite it as  $(\text{E}[N^1(n)]/n)/n$ . Note however, that the independence assumption is necessary for proving this bound. While in reality different results may not occur and co-occur truly independently, our experimental results in the evaluation results show our estimate works well in practice.

*Proof.* We will estimate the variance  $N^1(n)$  assuming independence of the different instances, We can express  $N^1(n)$  a sum of binary indicator variables  $X_i$ , which are 1 if instance  $i$  has shown up exactly once.  $X_i = 1$  with probability  $\pi_i(n) = np_i(1-p_i)^{n-1}$ . Then, because of our independence assumption, the total variance can be estimated by summing. Therefore  $N^1(n) = \sum_i X_i$  and because of our independence assumption  $\text{Var}[N^1(n)] = \sum_i \text{Var}[X_i]$ . Because  $X_i$  is a Bernoulli random variable, its variance is  $\pi_i(n)(1-\pi_i(n))$  which is bounded by  $\pi_i(n)$  itself. Therefore,  $\text{Var}[N^1(n)] \leq \sum n\pi_i(n)$ . This latter sum we know from before is  $\text{E}[N^1(n)]$ . Therefore  $\text{Var}[N^1(n)/n] \leq \text{E}[N^1(n)]/n^2$ .  $\square$

In fact, we can go further and fully characterize the distribution of values  $N^1(n)$  takes.

**Theorem (Sampling distribution of  $N^1(n)$ ).** *Assuming  $p_i$  are small or  $n$  is large, and assuming independent occurrence of instances,  $N^1(n)$  follows a Poisson distribution with parameter  $\lambda = \sum \pi_i(n)$ .*

*Proof.* We prove this by showing  $N^1(n)$ 's moment generating function (MGF) matches that of a Poisson distribution with  $\lambda$ ,  $M(t) = \exp(\lambda[e^t - 1])$ .

As in the proof of Equation 11, we think of  $N^1(n)$  as a sum of independent binary random variables  $X_i$ , one per instance. Each of these variables has a moment generating function  $M_{X_i}(t) = 1 + \pi_i(e^t - 1)$ . Because  $1 + x \approx \exp(x)$  for small  $x$ , and  $\pi_i(e^t - 1)$  will be small, then  $1 + \pi_i(e^t - 1) \approx \exp(\pi_i(e^t - 1))$ . Note  $\pi_i(e^t - 1)$  is always eventually small for some  $n$  because  $\pi_i(n + 1) = p_i(1 - p_i)^n \leq p_i e^{-np_i} \leq 1/en$ .

Because the MGF of a sum of independent random variables is the product of the terms' MGFs, we arrive at:  $M_{N^1(n)} = \prod_i M_{X_i}(t) = \exp([\sum_i \pi_i] [e^t - 1])$ .  $\square$

### 3.4.1 Thompson Sampling

Now we can use this bound to design a sampling strategy. The goal is to pick between  $(N_j^1(n), n_j)$  and  $(N_k^1(n), n_k)$  instead of only between  $N_j^1$  and  $N_k^1$ , where the only reasonable answer would be to pick the largest. One way to implement this comparison is to randomize it, which is what Thompson sampling [32] does.

Thompson sampling works by modeling unknown parameters such as  $R_j$  not with point estimates such as  $N_j^1(n_j)/n_j$  but with a wider distribution over its possible values. The width should depend on our uncertainty. Then, instead of using the point estimate to guide decisions, we use a sample from from this distribution. This effectively adds noise to our point estimate in proportion to how uncertain it is. In our implementation, we choose to model the uncertainty around  $R_j(n + 1)$  as following a Gamma distribution:

$$R_j(n + 1) \sim \Gamma(\alpha = N_j^1, \beta = n_j) \quad (12)$$

A Gamma distribution is shaped much like the Normal when the  $N^1/n$  is large, but behaves more like a single-tailed distribution when  $N^1/n$  is near 0, which is desirable because  $N^1/n$  will become very small over time, but we know our hidden  $\lambda$  is always non-negative. The Gamma distribution is a common way to model the uncertainty around an unobservable parameter  $\lambda$  for a Poisson distribution whose samples we can observe. Because we have shown that  $N^1(n)$  does in fact follow a Poisson distribution with an unknown parameter, this choice is especially suitable for our use case. The mean value of the Gamma distribution Equation 12 is  $\alpha/\beta = N_j^1/n_j$  which is by construction consistent with Equation 7, and its variance is  $\alpha/\beta^2 = N_j^1/n_j^2$  which is by construction consistent with the variance bound of Equation 11.

Finally, the Gamma distribution is not defined when  $\alpha$  or  $\beta$  are 0, so we need both a way to deal with the scenario where  $N^1(n) = 0$  which could happen often due to objects being rare, or due to having exhausted all results. As well as at initialization, when both  $N^1$  and  $n$  are 0. We do this by adding a small quantity  $\alpha_0$  and  $\beta_0$  to both terms, obtaining:

$$R_j(n_j + 1) \sim \Gamma(\alpha = N_j^1(n_j) + \alpha_0, \beta = n_j + \beta_0) \quad (13)$$

We used  $\alpha_0 = .1$  and  $\beta_0 = 1$  in practice, though we did not observe a strong dependence on this value. We experimented with alternatives to Thompson sampling, specifically Bayes-UCB [19], which uses upper quantiles from Equation 13 instead of samples to make decisions, but we did not observe significantly different results.

### 3.4.2 Empirical Validation

In this section we provide an empirical validation of the estimates from the previous sections, including Equation 7, and Equation 13. The question we are interested in is: given

an observed  $N^1$  and  $n$ , what is the true expected  $R(n + 1)$ , and how does it compare to the belief distribution  $\Gamma(N^1, n)$  which we propose using.

We ran a series of simulation experiments. To do this, we first generate 1000  $p_0, p_1, \dots, p_{1000}$  at random to represent 1000 results with different durations. To ensure there is duration skew we observe in real data, we use a lognormal distribution to generate the  $p_i$ . To illustrate the skew in the values, the smallest  $p_i$  is  $3 \times 10^{-6}$ , while the max  $p_i = .15$ . The median  $p_i$  is  $1 \times 10^{-3}$ . The parameters  $\mu_p$  computed from the  $p_i$  are  $3 \times 10^{-3}$  and  $8 \times 10^{-3}$  respectively. For a dataset with 1 million frames (about 10 hours of video), these durations correspond to objects spanning from 1/10 of a second up to about 1.5 hours, more skew than what normally occurs.

Then, we model the sampling of a random frame as follows: each instance is in the frame independently at random with probability  $p_i$ . To decide which of the instances will show up in our frame we simulate tossing 1000 coins independently, each with their own  $p_i$ , and the positive draws give us the subset of instances visible in that frame. We then proceed drawing these samples sequentially, tracking the number of frames we have sampled  $n$ , how many instances we have seen exactly once,  $N^1$ , and we also record  $E[R(n + 1)]$ : the expected number of new instances we can expect in a new frame sampled, which is possible because we can compute it directly as  $\sum_i^N [i \notin \text{seen}(n)] \cdot p_i$ , because in the simulation we know the remaining unknown instances and know their hidden probabilities  $p_i$ , so we compute  $E[R(n + 1)]$ . We sequentially sample frames up to  $n = 180000$ , and repeat the experiment 10K times, obtaining hundreds of millions of tuples of the form  $(n, N^1, R(n + 1))$  for our fixed set of  $p_i$ . Using this data, we can answer our original question: given an observed  $N^1$  and  $n$ , what is the true expected  $R(n + 1)$ ? by selecting different observed  $n$  and  $N^1$  at random, and conditioning (filtering) on them, plotting a histogram of the actual  $R(n + 1)$  that occurred in all our simulations. We show these histograms for 10 pairs of  $n$  and  $N^1$  in Figure 2, alongside our belief distribution.

Figure 2 shows a mix of 3 important scenarios. The first 3 subplots with  $n \leq 100$ , representative of the early stages of sampling. Here we see that the  $\Gamma$  model has substantially more variance than the underlying true distribution of  $R(n + 1)$ . This is intuitively expected, because early on both the bias and the variance of our estimate are bottlenecked by the number of samples, and not by the inherent uncertainty of  $R(n + 1)$ . As  $n$  grows to mid range values (next 4 plots), we see that the curve fits the histograms very well, and also that the curve keeps shifting left to lower and lower orders of magnitude on the x axis. Here we see that the one-sided nature of the Gamma distribution fits the data better than a bell shaped curve. The final 3 subplots show scenarios where  $n$  has grown large and  $N^1$  potentially very small, including a case where  $N^1 = 0$ . In that last subplot, we see the effect of having the extra  $\alpha_0$  in Equation 13, which means Thompson sampling will continue producing non-zero values at random and we will eventually correct our estimate when we find a new instance. In 3 of the subplots there is a clear bias to overestimate, though not that large despite the large skew.

This empirical validation was based on simulated data. In our evaluation we show these modeling choices work well in practice on real datasets as well, where our assumption of independence is not guaranteed and where durations may

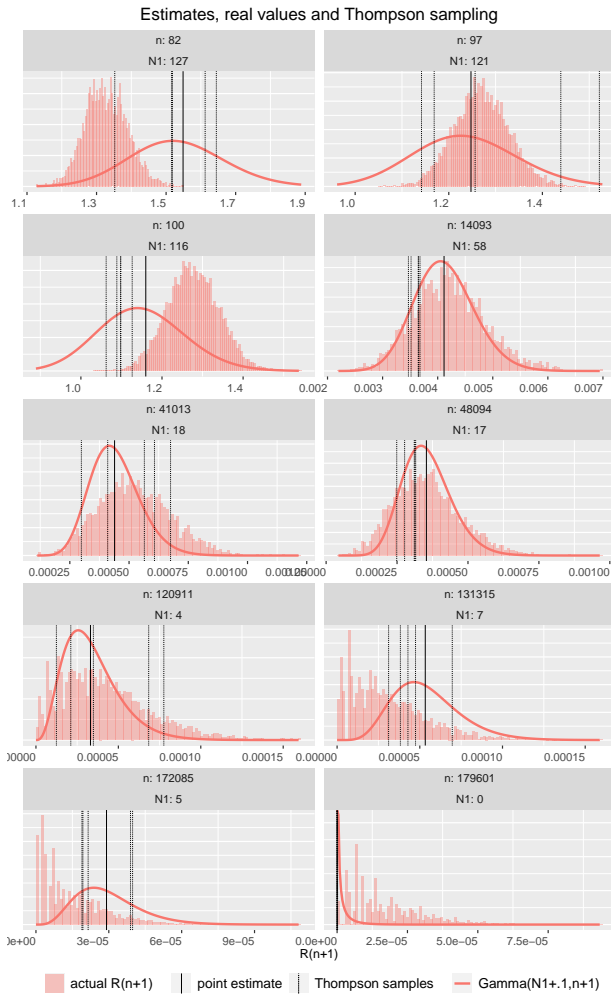


Figure 2: Comparing our Gamma heuristic of Equation 13 with a histogram of the true values  $R(n+1)$  from a simulation with heavily skewed  $p_i$ . The details of the simulation are discussed in Section 3.4.2. The histograms show the range of values seen for  $R(n+1)$  when we have the observed  $N^1$  and  $n$ . The point estimate  $N^1/n$  of (Equation 7) is shown as a vertical line. The belief distribution density is plotted as a thicker orange line, and 5 samples drawn using Thompson sampling are shown with dashed lines.

not necessarily follow the same distribution law.

### 3.5 Algorithm

The pseudocode for ExSample is shown in Algorithm 1. The inputs to the algorithm are:

- **video**: The video dataset itself, which may be a single video or a collection of files.
- **chunks**: The collection of logical chunks that we have split our video dataset into. There are  $M$  chunks total.
- **detector**: An object detector that processes video frames and returns object detections relevant to the query.
- **discrim**: The discriminator function that decides whether a detection is new or redundant.
- **result\_limit**: The limit clause indicating when to stop.

After initializing arrays to hold per-chunk statistics, the code can be understood in three parts: choosing a frame,

```

input : video, chunks, detector, discrim, result_limit
output: ans
1 ans  $\leftarrow$  []
   // arrays for stats of each chunk
2  $N^1 \leftarrow [0,0,\dots,0]$ 
3  $n \leftarrow [0,0,\dots,0]$ 
4 while len(ans) < result_limit do
   // 1) choice of chunk and frame
5   for  $j \leftarrow 1$  to  $M$  do
6      $R_j \leftarrow \Gamma(N^1[j] + \alpha_0, n[j] + \beta_0).sample()$ 
7   end
8    $j^* \leftarrow \arg \max_j R_j$ 
9   frame_id  $\leftarrow$  chunks[ $j^*$ ].sample()
   // 2) io, decode, detection and matching
10  rgb_frame  $\leftarrow$  video.read_and_decode(frame_id)
11  dets  $\leftarrow$  detector(rgb_frame)
   //  $d_0$  are the unmatched dets
   //  $d_1$  are dets with only one match
12   $d_0, d_1 \leftarrow$  discrim.get_matches(frame_id, dets)
   // 3) update state
13   $N^1[j^*] \leftarrow N^1[j^*] + \text{len}(d_0) - \text{len}(d_1)$ 
14   $n[j^*] \leftarrow n[j^*] + 1$ 
15  discrim.add(frame_id, dets)
16  ans.add( $d_0$ )
17 end

```

Algorithm 1: ExSample

processing the frame, and updating the sampler state. First, ExSample decides which frame to process next. It applies the Thompson sampling step in line 6, where we draw a separate sample  $R_j$  from the belief distribution Equation 13 for each of the chunks, which is then used in line 8 to pick the highest scoring chunk. The  $j$  in the code is used as the index variable for any loop over the chunks. During the first execution of the **while** loop all the belief distributions are identical, but their samples will not be, breaking the ties at random. Once we have decided on a best chunk index  $j^*$ , we sample a frame index at random from the chunk in line 9.

Second, ExSample reads and decodes the chosen frame, and applies the object detector on it (line 11). Then, we pass the computed detections on to a discriminator, which compares the detections with objects we have returned earlier during processing in other frames, and decides whether each detection corresponds to a new, distinct object. The discriminator returns two subsets:  $d_0$ , the detections that did not match with any previous results (are new objects), and  $d_1$ , the detections that matched exactly once with any previous detection. We will only use the size of those sets to update our statistics in the next stage. This frame processing stage of ExSample is the main bottleneck, and is dominated first by the detector call in line 11, and second by the random read and decode in line 10.

Third, we update the state of our algorithm, updating  $N^1$  and  $n$  for the chunk we sampled from. We also store detections in the discriminator and append the new detections to the result set (ans). We note that the amount of state we need to track only grows with the number of results we have output so far, and not with the size of the dataset.

### 3.6 Other Optimizations

We now extend Algorithm 1 with two optimizations.

**Batched execution.** Algorithm 1 processes one frame at a time, but on modern GPUs, inference is much faster when performed on batches of images. The code for a batched version is similar to that in Algorithm 1, but on line 6 we draw  $B$  samples per  $j$ , instead of one sample from each belief distribution, creating  $B$  cohorts of samples. In Figure 2 we show 5 different values from Thompson sampling of the same distribution in dashed lines. Because each sample for the same chunk will be different, the chunk with the maximum value will also vary and we will get  $B$  chunk indices, biased toward the more promising chunks. The logic for state update only requires small modifications. In principle, we may fear that picking the next  $B$  frames at random instead of only 1 frame could lead to suboptimal decision making within that batch, but at least for small values of  $B$  up to 50, which is what we use in our evaluation, we saw no significant drop. This batch size is sufficient to fully utilize a machine with 4 GPUs.

We do not implement or evaluate asynchronous, distributed execution in this paper, but the same reasoning suggests ExSample could be made to scale to an asynchronous setting, with workers processing a batch of frames without waiting for other workers. Ultimately, all the updates to  $N_j^1$  and  $n_j$  are commutative because they are additive.

**Avoiding near duplicates within a single chunk.** While random sampling is both a reasonable baseline and a good method for sampling frames within selected chunks, random allows samples to happen very close to each other in quick succession: for example in a 1000 hour video, random sampling is likely to start sampling frames within the same one hour block after having sampled only about 30 different hours, instead of after having sampled most of the hours once. For this reason, we introduce a variation of random sampling, which we call **random+**, to deliberately avoid sampling temporally near previous samples when possible: by sampling one random frame out of every hour, then sampling one frame out of every not-yet sampled half an hour at random, and so on, until eventually sampling the full dataset. We evaluate the separate effect of this change in our evaluation. We also use **random+** to sample within a chunk in ExSample, by modifying the internal implementation of the `chunk.sample()` method in line 9.

## 4. ANALYSIS

We have explained how ExSample allocates samples across chunks. In this section, we develop an analytical model to help us understand the circumstances under which our method performs better than random.

### 4.1 Upper Bound on Chunking Effectiveness

After  $n$  samples, ExSample will have allocated those samples across  $M$  different chunks, effectively weighting each chunk differently. In this section we derive an equation parameterized by dataset statistics to derive an upper bound on how well any method that allocates samples across chunks can do in terms of samples taken versus random sampling across the entire data set.

The number of results discovered by random sampling after  $n$  samples follows the curve

$$N(n) = \sum (1 - (1 - p_i)^n) = N - \sum (1 - p_i)^n \quad (14)$$

If we split the dataset into  $M$  chunks, then instead of having a single  $p_i$  of being found, instance  $i$  has a vector  $\mathbf{p}_i$  of  $M$  entries  $p_{ij}$ , where  $p_{ij}$  is the conditional probability of instance  $i$  being found in a sample on chunk  $j$ . Every weighted sampling scheme over these chunks corresponds to a  $M$  dimensional vector  $\mathbf{w}$  where  $w_j$  is the probability of sampling from chunk  $j$ . The total chance of sampling instance  $i$  under  $\mathbf{w}$  is the dot product  $\mathbf{p}_i \mathbf{w}$ . Hence,  $N(n, \mathbf{w}) = N - \sum (1 - \mathbf{p}_i \mathbf{w})^n$ . The optimal allocation of samples to chunks corresponds to the convex problem:

$$N^*(n) = N - \min_{\mathbf{w}} \sum (1 - \mathbf{p}_i \mathbf{w})^n \quad (15)$$

$$\text{subject to } \mathbf{w} \geq 0 \text{ and } \sum w_i = 1. \quad (16)$$

If we assume the  $M$  chunks are equally sized, then random sampling corresponds to  $\mathbf{w} = \mathbf{1}/M$ , and so it is only one of the feasible solutions, which makes clear that optimal weighted sampling is never worse than random sampling, though some implementations of weighted sampling could perform worse than random if weights are chosen poorly.

Note that ExSample does not have access to the  $\mathbf{p}_i$  ahead of time, instead ExSample is solving the same optimization problem but in an online fashion. However, for evaluation purposes in this paper, this bound can be computed directly from the  $\mathbf{p}_i$  using a solver package such as `cvxpy`[4], which is what we do in later sections. This bound is useful because once chunks are fixed, no method that relies on weighted random sampling can do better than this curve in expectation, this includes design variations of ExSample using different estimators, or different ways to model uncertainty. We later show empirically that ExSample converges to this bound, depending partially on our choice of chunks.

### 4.2 Data Dependent Parameters

The previous section provided a tight upper bound  $N^*(n)$  for any weighted sampling strategy, but it does not guarantee ExSample or even  $N^*(n)$  is always better than random sampling. This section explores how different parameters, in particular skew in instances and average duration of instances, affect ExSample performance in simulation.

Instance skew is a key parameter governing performance of ExSample. If we knew 95% of our results lie on the first half of the dataset, then we could allocate all our samples to that first half. This would boost the  $p_i$  of those results in the first half by  $2\times$ , without requiring knowledge of their precise locations. Hence we could expect about a  $2\times$  savings in the frames needed to reach the same number of results. Skew arises in datasets whenever the occurrence of an event correlates relevant latent factor that varies across time e.g., time of day or location (city, country, highway, camera angle) where video is taken. Note that ExSample does not know of these correlated factors or expect them as inputs in any way, but exploits this skew via sampling when it exists in the data.

In our simulation we show that under a wide variety of situations ExSample can outperform random by  $2x$  to  $80x$ , and it never does significantly worse. We also explore in detail situations random is competitive with ExSample. Results are shown in Figure 3.

To run the simulation, we fixed the number of instances  $N$  to 2000, and the number of frames to 16 million. We placed these 2000 instances according to a normal distribution centered in these 16 million frames, varying the standard deviation

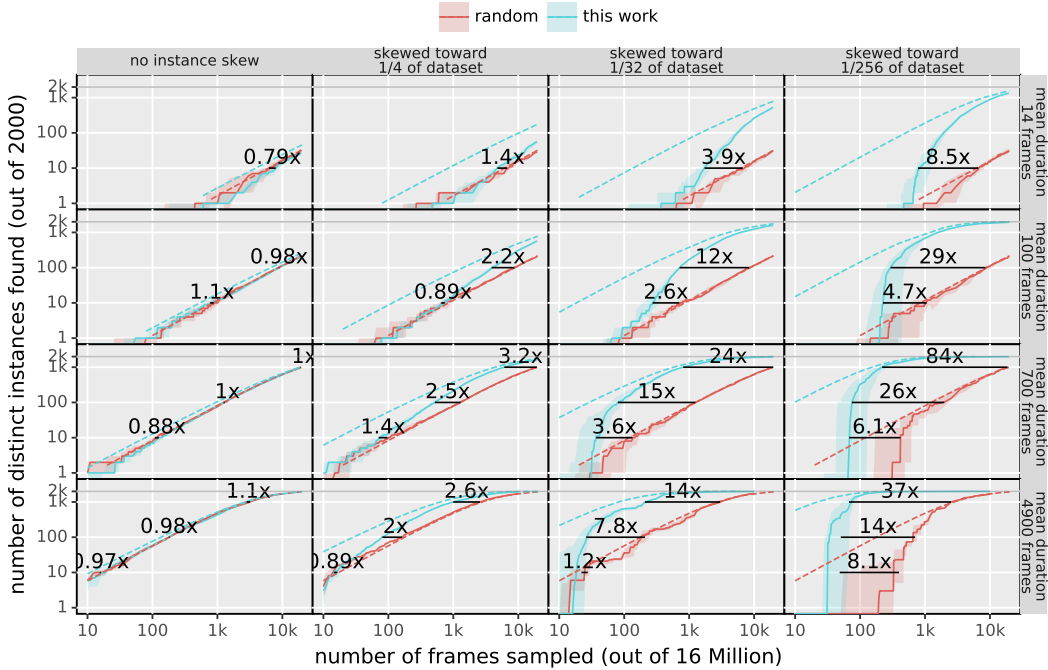


Figure 3: Simulated savings in frames from ExSample range from 1x to 84x depending on instance skew (increasing skew from left to right, starting with no skew), and on the average duration of a instance in frames (increasing from top to bottom). Solid lines show the median frames sampled by ExSample and random. Shaded areas mark 25-75 percentile. We label with text the savings in samples needed to reach 10, 100 and 1000 results. The dashed blue line show the expected results if samples were allocated optimally based on perfect prior knowledge of chunk statistics. The dashed red line shows the expected results from random. For a complete explanation see Section 4.2.

tion to result in no skew (left column in the figure) and skew where 95% of the instances appear in the center 1/4, 1/32, and 1/256 of the frames (additional columns in the figure). To generate varied durations for each of these instances, we use a LogNormal distribution with a target mean of 700 frames. This creates a set of durations where the shortest one is around 50 frames and the longest is around 5000 frames. To change the average duration we simply multiply or divide all durations by powers of 7, to get average durations of  $700/49 = 14$ ,  $700/7 = 100$ , 700,  $700 \times 7 = 4900$ . These correspond to the rows in Figure 3.

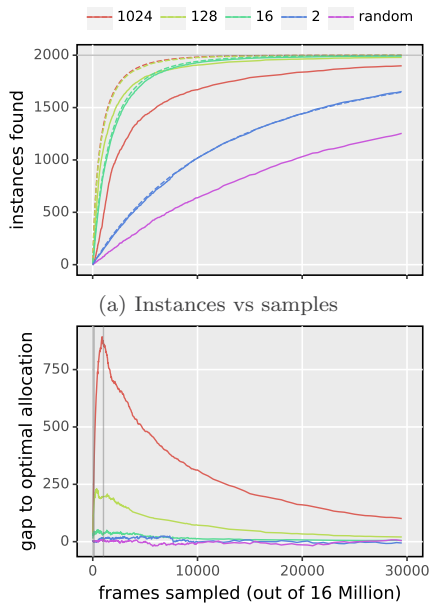
Once we have fixed these parameters, the different algorithms proceed by sampling frames, and we track the instances that have been found (y axis of subplots) as we increase the number of samples we have processed (x axis). For ExSample, we divide the frames into 128 chunks. We run each experiment 21 times. In Figure 3 we show the median trajectory (solid line) as well as a confidence band computed from the 25th to the 75th percentile (shaded). Additionally, the dashed lines show the expectation estimates computed using the formula in Equation 14. ExSample and random start off similarly, which is expected because we ExSample starts by sampling uniformly at random, but as samples accumulate, ExSample’s trajectory moves more and more toward the dashed blue line which represents the expected number of instances if the allocation of samples across chunks had been optimal from the beginning. ExSample outperforms random but performs similarly in two cases: 1) when there is very little skew in the locations of results (top row of figure) and 2) when results are very rare, which makes getting to the first result equally hard for both (left column of figure).

### 4.3 Chunks

The way we split the dataset into chunks is an external parameter that affects the performance of ExSample. We consider two extremes. Suppose we have a single chunk. This makes ExSample equivalent to random sampling. The fewer chunks there are, the less able to exploit any skew there is. Using two chunks imposes a hard ceiling on savings of  $2x$ , even if the skew is much larger, in this case 32. On the opposite extreme, one chunk per image frame would also be equivalent to random sampling: we would only sample from each chunk once before running out of frames, and we would not be able to use that that information to inform the following samples.

In Figure 4 we show how ExSample behaves for a range of chunk scenarios spanning several orders of magnitude. In this simulation, we fix instance skew (32) and  $p_i$  (with a mean duration of 700 frames), corresponding to the third column and third row of Figure 3. We vary the number of chunks from 1 to 1024. Dash lines show the optimal allocation from Equation 15; these lines improve with more chunks because we have exact knowledge of frame distribution and can exploit skew at smaller time scales. Note that a linear increase in chunks does not result in linear speedup, because the underlying instance skew is limited.

Solid lines in Figure 4 show the median performance of ExSample under different chunk settings. Here, increasing the number of chunks can decrease performance: for example going from 128 to 1024 chunks shows a decrease, even though both have similar optimal allocation (dashed) curves. The reason for this drop is that as we increase the number of chunks, we also increase the number of samples ExSample needs to be able to tell which chunks are more promising: when working with 1024 chunks, we need at least



(b) Vertical gap between dashed and solid lines

Figure 4: Varying the number of chunks for a fixed workload. Different colors correspond to different number of chunks in the legend. Dashed lines correspond to optimal sample allocation. Solid lines correspond to simulation results.

1024 samples for each chunk to be sampled once. During that time, ExSample performs like random.

The bottom subplot in Figure 4 presents the vertical gap between the dashed line and the solid line in the top subplot. We can see indeed that the gap peaks at around the time the number of samples reaches the number of chunks  $n = M$  and decreasing afterwards.

Thus, more chunks  $M$  can help improve how much of the instance skew any weighted sampling can exploit, but also implies a larger exploration "tax", proportional to  $M$ . For ExSample, this trade off shows up as a longer time to converge to the optimal allocation trajectory with larger  $M$ . We note, however that this sensitivity to chunks is not large – in our simulation we vary the number of chunks by 3 orders of magnitude and we still see a benefit of chunking versus random across all settings.

## 5. EVALUATION

Our goals for this evaluation are to demonstrate the benefits of ExSample on real data, comparing it to alternatives including random sampling as well as existing work in video processing. We show on these challenging datasets ExSample achieves savings of up to 4x with respect to random sampling, and orders of magnitude higher to approaches based on specialized surrogate models.

### 5.1 Experimental Setup

**Baselines.** We compare ExSample against two of the baselines discussed in Section 2.2: uniform random sampling and BlazeIt [17]. BlazeIt is the state-of-the-art representative of surrogate model methods for distinct object limit queries, and optimizes these queries by first performing a full scan of the dataset to compute surrogate scores on every video frame, and then processing frames from highest

to lowest score through the object detector. As in our approach, BlazeIt uses an object tracker to determine whether each computed detection corresponds to a distinct object.

**Implementation.** Our implementations of random sampling, BlazeIt, and ExSample are at their core sampling loops where the choice of which frame to process next is based on an algorithm-specific score. Based on this score, the system will fetch a batch of frames from the video and run that batch through an object detector. We implement this sampling loop in Python, using PyTorch to run inference on a GPU. For the object detector, we use FasterRCNN with a ResNet-50 backbone. To achieve fast random access frame decoding rates, we use the Hwang library from the Scanner project[30], and re-encode our video data to insert keyframes every 20 frames.

We implemented the subset of BlazeIt that optimizes distinct object limit queries, based on the description in the paper [17] as well as their published code. We opted for our own implementation to make sure the I/O and decoding components of both ExSample and BlazeIt were equally optimized, and also because extending BlazeIt to handle our own datasets and metrics was infeasible. For BlazeIt’s cheap surrogate model, we use an ImageNet pre-trained ResNet-18. This model is more expensive than the ones used in that paper, but also more accurate. Note that our timed results do not depend strongly on the inference cost of ResNet-18, since the model is still sufficiently lightweight that BlazeIt’s full scan is dominated by video IO and decoding time.

**Datasets.** We use 5 different datasets in this evaluation. Two datasets consist of vehicle-mounted dashboard camera video, while three datasets are from static street cameras.

The dashcam dataset consists of 10 hours of video, or over 1.1 million video frames, collected from a dashcam over several drives in cities and highways. Each drive can range from around 20 minutes to several hours. The BDD dataset used for this evaluation consists of a subset of the Berkeley Deep Drive Dataset[35]. Our subset is made out of 1000 randomly chosen clips. Because the BDD dataset has a wider variety of locations (multiple cities) and is made up of 1000 40-second clips, the number of chunks is forced to be high for this dataset. So, even though both datasets come from dashcams, they are quite different from each other.

The other three datasets are taken from [17], and consist of video recorded by fixed cameras overlooking urban locations. They are named *archie*, *amsterdam* and *night-street*, and each consists of 3 segments of 10 hours each taken on different days. These datasets are used in the evaluations of several existing works on optimizing video queries on static camera datasets [12, 16].

**Queries.** Each dataset contains slightly different types of objects, so we have picked between 6 and 8 objects per dataset based on the content of the dataset. In addition to searching for different object classes, we also vary the limit parameter recall of 10%, 50% and 90%, where recall is the fraction of distinct instances found. These recall rates are meant to represent different kinds of applications: 10% represents a scenario where an autonomous vehicle data scientist is looking for a few test examples, whereas a higher recall like 90% would be more useful in an urban planning or mapping scenario where finding most objects is desired.

**Ground Truth.** None of the datasets have human-generated object instance labels that identify objects over time. Therefore we approximate ground truth by sequentially scanning every video in the dataset and running each frame through a reference object detector (we reuse the Faster-RCNN model that we apply during query execution). If any objects are detected, we match the bounding boxes with those from previous frames and resolve which correspond to the same instance. To match objects across neighboring frames, we employ an IoU matching approach similar to SORT [3]. IoU matching is a simple baseline for multi-object tracking that leverages the output of an object detector and matches detection boxes based on overlap across adjacent frames.

## 5.2 Results

Here we evaluate the cost of processing, in both time and frames, distinct object queries using ExSample, **random+** and BlazeIt. Because some classes are much more common than others, the absolute times and frame counts needed to process a query vary by many orders of magnitude across different object classes. It is easier to get a global view of cost savings by normalizing query processing times of ExSample and BlazeIt against that of **random**. That is, if **random** takes 1 hour to find 20% of traffic lights, and ExSample takes 0.5 hours to do the same, time savings would be 2 $\times$ . We also apply this normalization when comparing frames processed. In the first part of this section we cover results for dashcam are shown in Figure 5 and for bdd in Figure 6. We cover the remaining datasets later.

### 5.2.1 Dashcam Dataset Results

Overall, ExSample saves more than 3 $\times$  in frames processed vs **random**, averaged across all classes and different recall levels. Savings do vary by class, reaching savings of above 5x for the bicycle class in the dashcam dataset. In terms of frames we can see BlazeIt performs really well at recall of 10% in the dashcam dataset, reaching 10 $\times$  the performance of **random**. The reason is that in the dashcam dataset BlazeIt surrogate models learn to classify frames much better than random, as is evident in Figure 7. For high recall levels, however, this initial advantage diminishes because it is hard to avoid resampling the same instances in different frames, despite skipping a gap of 100 frames when a result is successfully found.

The story becomes more complex when comparing runtime. On the right panel of Figure 5 we show the total runtime costs, including overhead incurred prior to processing the query, which erase the early wins from better prediction on the left panel. The impact of this overhead reduces in magnitude as more samples are taken, and so the difference is less dramatic at higher recall levels. For BlazeIt the total time in the plot is a sum of three separate costs: those of training, scoring, and sampling. Training costs are mostly due to needing to label a fraction of the dataset using the expensive detector. Scoring costs come from needing to scan and process the full dataset with the surrogate model. Finally, sampling costs come from visiting frames in score order.

In Table 1 we quantify the costs of the three steps, where for BlazeIt we estimate sampling costs by assuming a well trained surrogate model finding instances 100 $\times$  faster than random. The table shows that BlazeIt’s runtime is dominated first by scoring (i.e., the full scan to process every

frame through the surrogate model), and second by labeling. While it may be possible to amortize the costs of labeling in BlazeIt across many queries, because the expensive model may provide general-purpose labels, the full scan that dominates the overhead cannot be amortized as the surrogate is query-specific. Because **random** does not need to scan the entire dataset before yielding results, it can afford to be much worse in precision while still providing a faster runtime, especially at low recalls. ExSample outperforms the other methods because it provides high sampling precision while avoiding the need for a full scan.

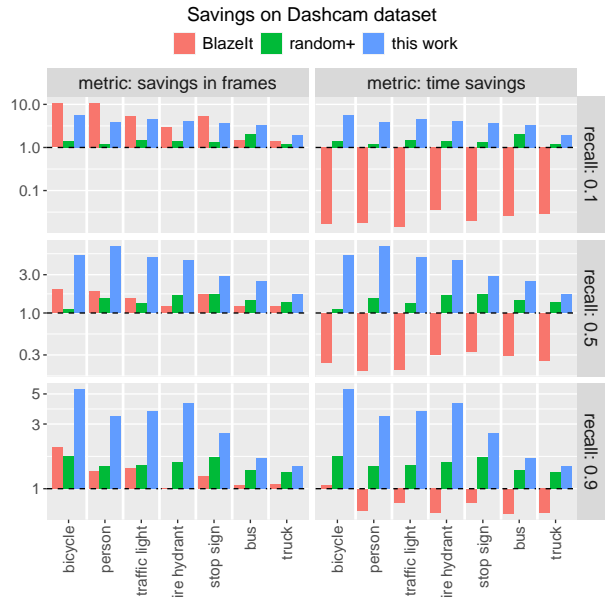


Figure 5: Results on the Dashcam dataset. Comparing frames (left column) and times(right column) for different recall levels (each row) on the dashcam dataset. Different methods (color) are compared relative to the costs of using **random** to process the same query and reach the same level of instance recall.

stage	throughput(fps)	BlazeIt frames/time(s)	random frames/time(s)
label	20	110K/5.8Ks	0
score	100	1.1M/12Ks	0
sample	20	120/5.8s	1.2K/58s

Table 1: Time breakdown: random vs BlazeIt.

### 5.2.2 BDD Results

The maximum benefit from ExSample is lower in Figure 6, reaching only 3x. BDD is a challenging scenario for ExSample because as we have mentioned earlier, it is composed of 1000 40 second clips. BDD is also challenging for BlazeIt, because surrogate models have a harder time learning with high accuracy on this dataset, which presents many points of view and small objects. Figure 7 shows that surrogate models do not reach particularly high Average Precision. This is not an issue for ExSample because we do not rely on a cheaper approximation, which may not be as easy to get for highly variable datasets.

### 5.2.3 Additional Datasets

In addition to the Dashcam and BDD datasets, we evaluated ExSample on archie, amsterdam, and night-street from

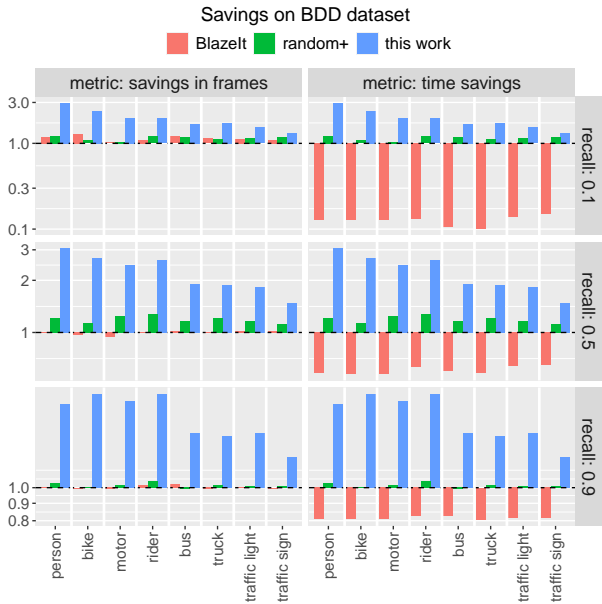


Figure 6: Results on BDD dataset. Surrogate has a harder time learning on this dataset, with lower accuracy scores. Counterintuitively, this makes its savings comparable to those of `random` sampling, improving its results compared to Dashcam dataset

the BlazeIt paper [17], and measured how ExSample performs compared to random in terms of frame savings on all five datasets. This evaluation includes around 35 classes total across the datasets. The results are aggregated below by dataset in Table 2 (averaging across recall levels) and by recall level in Table 4 (averaging across datasets).

Table 2 shows that savings are both query and data dependent. This is reflected in Figure 8, where we show an object for each dataset, and how its distribution is skewed across chunks in the dataset. The dataset/class combos with the largest skews (dashcam, bdd1k and night-street) also show the largest gains, as expected based on Section 4.2. Amsterdam and archie have little skew overall on any class, hence ExSample cannot perform much better than `random`. On BDD, there are many short chunks due to the dataset structure, so the savings are lower than skew would suggest, as explained in Section 4.3.

dataset	classes	min (savings)	median	max
dashcam	7	1.7	4.1	6.5
bdd1k	8	1.5	1.9	3.5
night-street	6	1.2	1.6	3.1
amsterdam	7	0.9	1.5	1.7
archie	6	1.2	1.4	1.5

Table 2: Aggregate savings of ExSample relative to random for the different datasets.

Rather than running a specific surrogate-based system like BlazeIt on these additional datasets, we compared ExSample to an idealized surrogate, which has a 100% recall on identifying instances, so its cost is just the cost it takes to score all frames in the dataset. We show how the fraction of instances that ExSample can identify in the time it takes this idealized surrogate do this scoring, using surrogate timing data based on the experiments in subsection 5.2, using the same five classes show in Figure 8. The results are shown in Table 3. From this, we can see that across a range of object

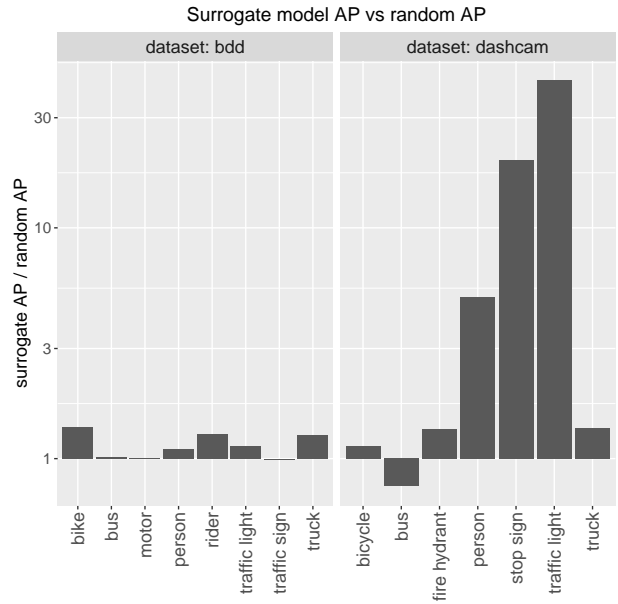


Figure 7: Average Precision of surrogate models vs a randomly assigned score. For BDD, the surrogate model does only slightly better than random in precision, which causes it to perform similarly to random when measured in savings in Figure 6. For the Dashcam dataset, the surrogate models are more accurate than random. Counterintuitively, higher accuracy in scores hurts relative performance in Figure 5 due to the greediness of the algorithm.

dataset	category	recall (this work)	fraction sampled
A-dashcam	bicycle	0.72	0.07
B-bdd1k	motor	0.38	0.22
C-night street	person	0.90	0.02
D-archie	car	0.90	0.02
E-amsterdam	boat	0.90	0.02

Table 3: Recall level reached by ExSample in the same amount of time it would take to scan the dataset. The experiment stops at recall .9.

classes and skew, ExSample can detect most instances in a dataset before a surrogate can score all frames.

Finally, Table 4 compares ExSample to random on all 5 datasets, aggregating by recall. Here ExSample performs slightly better at 50% recall, because at 10% recall, with fewer samples, ExSample has had less time to identify chunks with more instances, and at 90% recall, some of the instances are in less skewed chunks that ExSample samples less.

recall	min (savings)	median	max
10%	0.8	1.4	6.9
50%	0.9	1.7	6.9
90%	1.2	1.9	4.8

Table 4: Aggregate savings broken down by recall.

## 6. RELATED WORK

**Video Data Management.** There has recently been renewed interest in developing data management systems for video analytics, motivated in large part by the high cost of applying state-of-the-art video understanding methods, which almost always involve expensive deep neural networks, on large datasets. Recent systems adapt prior work in visual

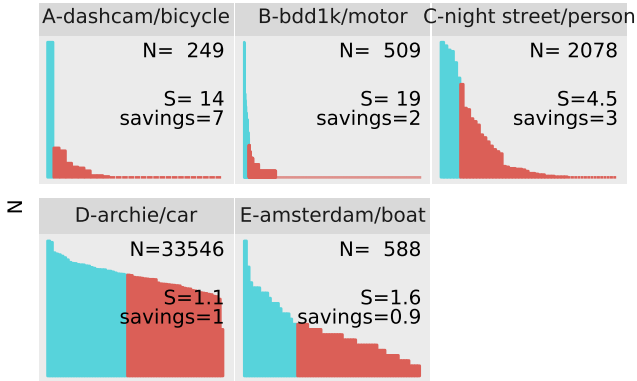


Figure 8: Instance skew and savings for different classes and datasets of Table 2. Each vertical bar corresponds to a chunk’s number of instances. The blue colored bars are the minimum set that cover 50% of instances.  $S$  is our skew metric defined in Section 4.2.

data management [5, 29] for modern tasks that involve applying machine learning techniques to extract insights from large video datasets potentially comprising of millions of hours of video. In particular, DeepLens [21] and VisualWorldDB [9] explore a wide range of opportunities that an integrated data management system for video data would enable. DeepLens [21] proposes an architecture split into storage, data flow, and query processing layers, and considers tradeoffs in each layer – for example, the system must choose from several storage formats, including storing each frame as a separate record, storing video in an encoded format, and utilizing a hybrid segmented file. VisualWorldDB proposes storing and exposing video data from several perspectives as a single multidimensional visual object, achieving not only better compression but also faster execution.

**Speeding up Video Analytics.** Several optimizations have been proposed to speed up execution of various components of video analytics systems to address the cost of mining video data. Many recent approaches train specialized surrogate classification models on reduced dimension inputs derived from the video [18, 24, 20, 12, 2]. As we detailed in Section 2.2, most related to our work is BlazeIt [17], which adapts surrogate-based video query optimization techniques for object search limit queries.

Video analytics methods employing surrogate models are largely orthogonal to our work: we can apply ExSample to sample frames, while still leveraging a cascaded classifier so that expensive models are only applied on frames where fast, surrogate models have sufficient confidence. The extensions to limit queries proposed to BlazeIt are not orthogonal, as they involve controlling the sampling method, but a fusion sampling approach that combines ExSample with BlazeIt may be possible. Nevertheless, a major limitation of BlazeIt is that it requires applying the surrogate model on every video frame even for limit queries; as we showed in Section 5, this presents a major bottleneck that can make BlazeIt slower on limit queries than random sampling.

Besides methods employing surrogate models, several approaches, such as Chameleon [16] as well as [14, 33, 34], consider tuning optimization knobs such as the neural network model architecture, input resolution, and sampling framerate to achieve the optimal speed-accuracy tradeoff. Like surrogate models, these approaches are orthogonal to ExSample

and can be applied in conjunction.

**Speeding up Object Detection.** Accelerating video analytics by improving model inference speed has been extensively studied in the computer vision community. Because these methods optimize speed outside of the context of a specific query, they are orthogonal to our approach and can be straightforwardly incorporated. Several general-purpose techniques improve neural network inference speed by pruning unimportant connections [8, 22] or by introducing models that achieve high accuracy with fewer parameters [11, 15]. Coarse-to-fine object detection techniques first detect objects at a lower resolution, and only analyze particular regions of a frame at higher resolutions if there is a large expected accuracy gain [6, 27]. Cross-frame feature propagation techniques accelerate object tracking by applying an expensive detection model only on sparse key frames, and propagating its features to intermediate frames using a lightweight optical flow network [36, 37].

## 7. CONCLUSION

Over the next decade, workloads that process video to extract useful information may become a standard data mining task for analysts in areas such as government, real estate, and autonomous vehicles. Such pipelines present a new systems challenge due to the cost of applying state of the art machine vision techniques over large video repositories.

In this paper we introduced ExSample, an approach for processing distinct object search queries on large video repositories through chunk-based adaptive sampling. Specifically, the aim of the approach is to find frames of video that contain objects of interest, without running an object detection algorithm on every frame, which is often prohibitively expensive. Instead, in ExSample, we adaptively sample frames with the goal of finding the most distinct objects in the shortest amount of time – ExSample iteratively processes batches of frames, tuning the sampling process based on whether new objects were found in the frames sampled on each iteration. To do this tuning, ExSample partitions the data into chunks and dynamically adjusts the frequency with which it samples from different chunks based on the rate at which new objects are sampled from each chunk. We formulate this sampling process as an instance of Thompson sampling, using a Good-Turing estimator to compute the per-chunk likelihood of finding a new object in a random frame. In this way, as objects in a particular chunk are exhausted, ExSample naturally refocuses its sampling on other less frequently sampled chunks.

Our evaluation of ExSample on a real-world dataset of dashcam video shows that it is able to substantially reduce both the number of sampled frames and the execution time needed to achieve a particular recall compared to both random sampling and methods based on lightweight surrogate models, such as BlazeIt [17], that are designed to estimate frames likely to contain objects of interest with lower overhead. Thus, we believe that ExSample represents a key step in building cost-efficient video data management systems.

## 8. REFERENCES

- [1] AWS. Amazon EC2 on-demand pricing. <https://aws.amazon.com/ec2/pricing/on-demand>. Accessed: 2020-09-10.

- [2] F. Bastani, S. He, A. Balasingam, K. Gopalakrishnan, M. Alizadeh, H. Balakrishnan, M. Cafarella, T. Kraska, and S. Madden. Miris: Fast object track queries in video. In *Proceedings of the 2020 ACM SIGMOD International Conference on Management of Data*, pages 1907–1921, 2020.
- [3] A. Bewley, Z. Ge, L. Ott, F. Ramos, and B. Upcroft. Simple online and realtime tracking. *CoRR*, abs/1602.00763, 2016.
- [4] S. Diamond and S. Boyd. CVXPY: A Python-embedded modeling language for convex optimization. *Journal of Machine Learning Research*, 17(83):1–5, 2016.
- [5] M. Flickner, H. Sawhney, W. Niblack, J. Ashley, Q. Huang, B. Dom, M. Gorkani, J. Hafner, D. Lee, D. Petkovic, et al. Query by image and video content: The QBIC system. *Computer*, 28(9):23–32, 1995.
- [6] M. Gao, R. Yu, A. Li, V. I. Morariu, and L. S. Davis. Dynamic zoom-in network for fast object detection in large images. In *Proceedings of the IEEE Conference on Computer Vision and Pattern Recognition*, pages 6926–6935, 2018.
- [7] I. J. GOOD. THE POPULATION FREQUENCIES OF SPECIES AND THE ESTIMATION OF POPULATION PARAMETERS. *Biometrika*, 40(3-4):237–264, 12 1953.
- [8] S. Han, H. Mao, and W. J. Dally. Deep compression: Compressing deep neural networks with pruning, trained quantization and huffman coding. In *International Conference on Learning Representations*, 2016.
- [9] B. Haynes, M. Daum, A. Mazumdar, M. Balazinska, A. Cheung, and L. Ceze. VisualWorldDB: A dbms for the visual world. In *CIDR*, 2020.
- [10] K. He, G. Gkioxari, P. Dollár, and R. B. Girshick. Mask R-CNN. *CoRR*, abs/1703.06870, 2017.
- [11] A. G. Howard, M. Zhu, B. Chen, D. Kalenichenko, W. Wang, T. Weyand, M. Andreetto, and H. Adam. MobileNets: Efficient convolutional neural networks for mobile vision applications. *CoRR*, abs/1704.04861, 2017.
- [12] K. Hsieh, G. Ananthanarayanan, P. Bodik, S. Venkataraman, P. Bahl, M. Philipose, P. B. Gibbons, and O. Mutlu. Focus: Querying large video datasets with low latency and low cost. In *13th {USENIX} Symposium on Operating Systems Design and Implementation ({OSDI} 18)*, pages 269–286, 2018.
- [13] J. Huang, V. Rathod, C. Sun, M. Zhu, A. Korattikara, A. Fathi, I. Fischer, Z. Wojna, Y. Song, S. Guadarrama, and K. Murphy. Speed/accuracy trade-offs for modern convolutional object detectors. *CoRR*, abs/1611.10012, 2016.
- [14] C.-C. Hung, G. Ananthanarayanan, P. Bodik, L. Golubchik, M. Yu, P. Bahl, and M. Philipose. VideoEdge: Processing camera streams using hierarchical clusters. In *2018 IEEE/ACM Symposium on Edge Computing (SEC)*, pages 115–131. IEEE, 2018.
- [15] F. N. Iandola, S. Han, M. W. Moskewicz, K. Ashraf, W. J. Dally, and K. Keutzer. SqueezeNet: AlexNet-level accuracy with 50x fewer parameters and 0.5 mb model size. *arXiv preprint arXiv:1602.07360*, 2016.
- [16] J. Jiang, G. Ananthanarayanan, P. Bodik, S. Sen, and I. Stoica. Chameleon: Scalable adaptation of video analytics. In *Proceedings of the 2018 Conference of the ACM Special Interest Group on Data Communication*, pages 253–266, 2018.
- [17] D. Kang, P. Bailis, and M. Zaharia. Blazeit: Fast exploratory video queries using neural networks. *CoRR*, abs/1805.01046, 2018.
- [18] D. Kang, J. Emmons, F. Abuzaid, P. Bailis, and M. Zaharia. NoScope: Optimizing neural network queries over video at scale. *Proc. VLDB Endow.*, 10(11):1586–1597, Aug. 2017.
- [19] E. Kaufmann. On bayesian index policies for sequential resource allocation. *Ann. Stat.*, 46(2):842–865, Apr. 2018.
- [20] N. Koudas, R. Li, and I. Xarchakos. Video monitoring queries. In *2020 IEEE 36th International Conference on Data Engineering (ICDE)*, pages 1285–1296. IEEE, 2020.
- [21] S. Krishnan, A. Dziedzic, and A. J. Elmore. Deeplens: Towards a visual data management system. In *Conference on Innovative Data Systems Research (CIDR)*, 2019.
- [22] G. Leclerc, R. C. Fernandez, and S. Madden. Learning network size while training with ShrinkNets. In *Conference on Systems and Machine Learning*, 2018.
- [23] T. Lin, M. Maire, S. J. Belongie, L. D. Bourdev, R. B. Girshick, J. Hays, P. Perona, D. Ramanan, P. Dollár, and C. L. Zitnick. Microsoft COCO: common objects in context. *CoRR*, abs/1405.0312, 2014.
- [24] Y. Lu, A. Chowdhery, S. Kandula, and S. Chaudhuri. Accelerating machine learning inference with probabilistic predicates. ACM SIGMOD, June 2018.
- [25] O. Moll, F. Bastani, S. Madden, M. Stonebraker, V. Gadepally, and T. Kraska. ExSample: Efficient searches on video repositories through adaptive sampling (technical report). <https://github.com/orc011/tmp/blob/master/techreport.pdf>, September 2020.
- [26] T. Murray. Help improve imagery in your area with our new camera lending program. <https://www.openstreetmap.us/2018/05/camera-lending-program/>, 2018.
- [27] M. Najibi, B. Singh, and L. S. Davis. Autofocus: Efficient multi-scale inference. In *Proceedings of the IEEE International Conference on Computer Vision*, pages 9745–9755, 2019.
- [28] Nexar. Nexar. <https://www.getnexar.com/company>, 2018.
- [29] V. E. Ogle and M. Stonebraker. Chabot: Retrieval from a relational database of images. *Computer*, 28(9):40–48, 1995.
- [30] A. Poms, W. Crichton, P. Hanrahan, and K. Fatahalian. Scanner: Efficient video analysis at scale. *ACM Trans. Graph.*, 37(4):138:1–138:13, July 2018.
- [31] J. Redmon and A. Farhadi. YOLOv3: An incremental improvement. *CoRR*, abs/1804.02767, 2018.
- [32] D. Russo, B. V. Roy, A. Kazerouni, and I. Osband. A

- tutorial on thompson sampling. *CoRR*, abs/1707.02038, 2017.
- [33] R. Xu, J. Koo, R. Kumar, P. Bai, S. Mitra, G. Meghanath, and S. Bagchi. ApproxNet: Content and contention aware video analytics system for the edge. *arXiv preprint arXiv:1909.02068*, 2019.
- [34] T. Xu, L. M. Botelho, and F. X. Lin. VStore: A data store for analytics on large videos. In *Proceedings of the Fourteenth EuroSys Conference*, pages 1–17, 2019.
- [35] F. Yu, W. Xian, Y. Chen, F. Liu, M. Liao, V. Madhavan, and T. Darrell. BDD100K: A diverse driving video database with scalable annotation tooling. *CoRR*, abs/1805.04687, 2018.
- [36] X. Zhu, J. Dai, L. Yuan, and Y. Wei. Towards high performance video object detection. In *Proceedings of the IEEE Conference on Computer Vision and Pattern Recognition*, pages 7210–7218, 2018.
- [37] X. Zhu, Y. Xiong, J. Dai, L. Yuan, and Y. Wei. Deep feature flow for video recognition. In *Proceedings of the IEEE Conference on Computer Vision and Pattern Recognition*, pages 2349–2358, 2017.